Main-Group Compounds

DOI: 10.1002/anie.201308888

Probing the Zintl–Klemm Concept: A Combined Experimental and Theoretical Charge Density Study of the Zintl Phase CaSi**

Iryna M. Kurylyshyn, Thomas F. Fässler, Andreas Fischer, Christoph Hauf, Georg Eickerling, Manuel Presnitz, and Wolfgang Scherer**

Abstract: *The nature of the chemical bonds in CaSi, a textbook example of a Zintl phase, was investigated for the first time by means of a combined experimental and theoretical charge density analysis to test the validity of the Zintl–Klemm concept. The presence of covalent Si–Si interactions, which were shown by QTAIM analysis, supports this fundamental bonding concept. However, the use of an experimental charge density study and theoretical band structure analyses give clear evidence that the cation–anion interaction cannot be described as purely ionic, but also has partially covalent character. Integrated QTAIM atomic charges of the atoms contradict the original Zintl–Klemm concept and deliver a possible explanation for the unexpected metallic behavior of CaSi.*

The Zintl–Klemm concept is based on Eduard Zintl's thoughts on the formation of salt-like intermetallic compounds in 1931[1] and culminated in 1939 in the description of NaTl[2] by a formal transfer of electrons from the more electropositive Na to Tl.[3] The description of the polyanionic Tl substructure in terms of a diamond structure type, representing a structural motif typically adopted by elements possessing four valence electrons and covalently bonded atoms, is a milestone in the understanding of certain intermetallic solids, namely the Zintl phases.[4] The structural description was originally based on the size of the anionic atoms and the idea that covalent bonds exist between the atoms of the anionic substructure gradually emerged. The original concept by Zintl was later extended by Klemm[5] and Laves[6] and has developed into a versatile and general concept.[7] In general, Zintl phases are regarded as compounds composed of electropositive metals A and electronegative metals or semimetals M (for example, p-block metals of Groups 13, 14, and 15), the structures of which can be understood by the formal electron transfer from A to M and the anionic substructure of M atoms obeying the 8–*N* octet rule.

Zintl phases should have filled conduction bands and display semiconducting behavior, although the prototype NaTl as well as many others show metallic properties.[8,9] This clearly indicates that the original Zintl–Klemm concept might still be too simplistic.[10] A major reason might be that the formal charge distribution does not reflect the real charge transfer.

Herein we will focus on the nature of chemical bonding in CaSi, a textbook example of a Zintl phase with respect to the 8–*N* rule, which displays peculiar chemical bonding.[11] Owing to the overuse of the term "Zintl phase", the primary goal of this contribution is to present for the first time experimental charge density analyses to validate the fundamental bonding concept of these phases. CaSi melts congruently at 1320 °C,[12] and the growth of single crystals of sufficient quality is possible. In accordance with the Zintl–Klemm concept, the anions form chains of two-bonded Si^{2-} atoms. These polyanionic $^{1}_{\infty}[Si^{2-}]$ chains parallel to the crystallographic *c* axis are stacked along the *a* axis and are separated by isolated Ca^{2+} atoms (Figure 1 a). However, they are not helical but planar, in contrast to the structure of the corresponding neutral iso(valence)electronic elemental structure of gray selenium.[13]

Electrical resistivity measurements and electronic structure calculations reveal metallic properties,[14] which can be attributed to the π character of the Si–Si bond. To elucidate

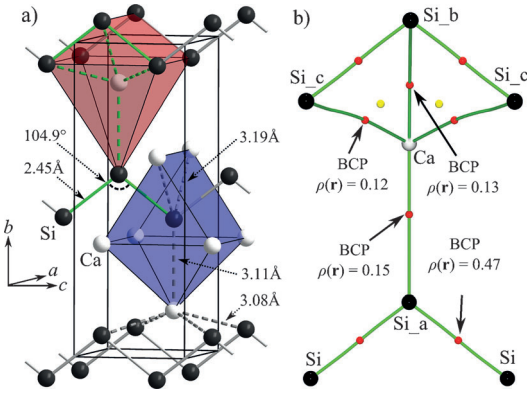

Figure 1. a) View of the CaSi structure with salient experimental distances and angles, Ca and Si atoms are drawn as light gray and black spheres, respectively. b) Experimental bond paths of the reference structural moiety as defined and highlighted in (a) by green bond sticks. Bond and ring critical points are marked by red and yellow spheres, respectively, and the corresponding density values are specified in $eÅ^{-3}$. Three different types of BCPs are formed between Ca and the symmetry-related Si atoms (Si_a-Si_c).

[*] M.Sc. I. M. Kurylyshyn, Prof. Dr. T. F. Fässler
Department of Chemistry, Technische Universität München
Lichtenbergstrasse 4, 85747 Garching (Germany)
E-mail: thomas.faessler@lrz.tum.de
M.Sc. A. Fischer, Dipl.-Phys. C. Hauf, Dr. G. Eickerling,
Dipl.-Phys. M. Presnitz, Prof. Dr. W. Scherer
Institut für Physik, Universität Augsburg
86135 Augsburg (Germany)
E-mail: wolfgang.scherer@physik.uni-augsburg.de

[**] This work has been supported by the Deutsche Forschungsgemeinschaft SPP 1178 project numbers FA 198/10-1 and SCHE 478/12-1.

Supporting information for this article is available on the WWW under http://dx.doi.org/10.1002/anie.201308888.

the highly anisotropic character, which is substantial for the covalent bonds between the Si atoms on one hand and the importance of Ca–Si bonds on the other, we apply here an analysis of the topology of the experimental electron density by the atoms in molecules (AIM) approach.[15] The experimental density distributions were obtained from high-resolution single-crystal X-ray diffraction experiments and subsequent multipolar refinements employing the Hansen–Coppens (HC) multipolar model.[16] Comparison with theoretically determined charge density distributions obtained from periodic full-potential LAPW DFT calculations provided substantial evidence from theory and experiment to classify CaSi as a true Zintl phase despite its well-established metallic character.

The distance between the Si atoms in the $^1_\infty[Si^{2-}]$ chain is 2.4515(1) Å and thus slightly longer than in elemental silicon (2.352 Å).[17] The coordination polyhedron of Si is composed of seven Ca atoms that form a distorted monocapped trigonal prism (highlighted in blue in Figure 1 a) with Si being located inside the trigonal prism. The first coordination sphere of Ca (highlighted in red in Figure 1 a) is built again of a distorted monocapped trigonal prism of Si atoms with Ca situated in the rectangular pyramid of the capped face. The three Si atoms of each of the two trigonal faces of the distorted trigonal prism are parts of two coplanar zigzag chains with Ca–Si distances of 3.08408(2) Å (4×) and 3.19286(6) Å (2×). The seventh Si atom that completes the rectangular pyramid (and caps the distorted trigonal prism) completes the Ca coordination sphere with a Ca–Si distance of 3.11066(9) Å.[18]

Figure 2 a,b depict the experimental and theoretical deformation electron density distributions in the plane spanned by a $^1_\infty[Si^{2-}]$ zigzag chain. Charge accumulations in the Si–Si and the Ca–Si bonding domains reflect the covalent character of the Si–Si bond but surprisingly also signal the presence of noticeable covalent Ca–Si interactions. This result is supported by a topological analysis of the electron density distribution, which reveals the presence of Si–Si and Ca–Si bond paths within this plane (Figure 1 b and 2 c). It can already be seen at this stage that the valence shell of the calcium atom is significantly polarized. This phenomenon is, however, less pronounced in case of the experimental model owing to the limitation of the resolution of our diffraction study ($d > 0.36$ Å). We will outline at a later stage that the characteristic polarization of the calcium atom is inherently linked with the involvement of metal d states in the Ca–Si bonding interaction.

In the following, topological parameters obtained from theoretical LAPW densities will be specified in square brackets. Inspection of the topology of the total electron density at the Si–Si bond critical points (BCPs) classifies this bond as predominantly covalent owing to its pronounced density accumulation of $\rho(\mathbf{r}_c) = 0.47$ [0.44] e Å^{-3}. This conclusion is further supported by the negative sign of the Laplacian of the electron density (Figure 2 c) at the Si–Si BCPs ($\nabla^2\rho(\mathbf{r}_c) = -1.31$ [−1.28] e Å^{-5}) and of the local energy density ($H(\mathbf{r}_c) = -0.23$ [−0.26] Hartree Å^{-3});[19] values given for theory and experiment, respectively. In comparison to α-Si [$\rho(\mathbf{r}_c) = 0.56$ e Å^{-3}],[20] the Si–Si bond strength in the $^1_\infty[Si^{2-}]$ zigzag chain of CaSi appears to be significantly decreased, in

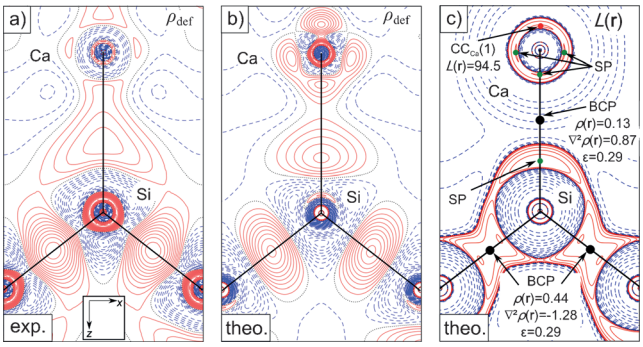

Figure 2. a) Experimental and b) theoretical deformation electron density plotted in the plane of the $^1_\infty[Si]$ zigzag chains that denotes our local *xz* coordinate system. The density contours (positive and negative values shown as solid red and dashed blue lines, respectively) are equally spaced by increments of 0.01 e Å^{-3}. c) Theoretical $L(\mathbf{r}) = -\nabla^2\rho(\mathbf{r})$ map, showing the Ca–Si and Si–Si bond paths. Positive (solid red) and negative (dashed blue) contour lines were drawn at $\pm 2.0\times10^n$, $\pm 4.0\times10^n$, $\pm 8.0\times10^n$ e Å^{-5} with $n = \pm 2, \pm 1, 0$. Extra contour lines are drawn at 1.55 e Å^{-5} and 88 e Å^{-5} (80 e Å^{-5} omitted); Charge concentrations and saddle points in $L(\mathbf{r})$ are shown as red and green points, while BCPs are denoted by black spheres. Units are e Å^{-3} for $\rho(\mathbf{r})$ and e Å^{-5} for $L(\mathbf{r})$ and $\nabla^2\rho(\mathbf{r})$. Note that theoretical density and $L(\mathbf{r})$ contour maps have been obtained by modeling of the theoretical Wien2K structure factors by a highly flexible multipolar model (for details, see the Supporting Information, Figures S1 and S8).

line with the elongated Si–Si bond distances. This observation hints already to the more delocalized nature of the valence density distribution inside the zigzag chains, which might be the physical origin of the remarkable metallic properties in CaSi. Also the unusual planar structure of the $^1_\infty[Si^{2-}]$ chains supports their delocalized nature and hints towards a formal sp^2 hybridization of the silicon. The assumed π-character of these zigzag chains is indeed supported by the pronounced bond ellipticity ε of 0.14 [0.29] at the Si–Si bond critical points (BCPs; Figure 3 a and Supporting Information, Table S9). According to the mathematical definition (see Caption of Figure 3), these ε values greater than zero clearly indicate electronic distortions away from σ-symmetry, such as a partial π-character along the Si–Si bond path.

The analysis of the band structure of CaSi further supports this assumption. The site- and state-projected band structure plots ("fat bands") of the Si p_y and p_z states are shown in

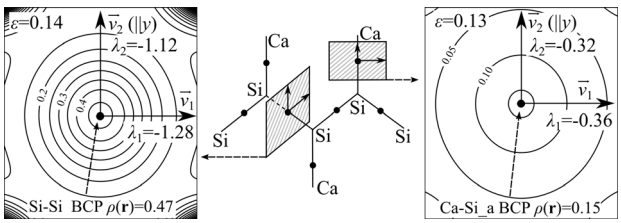

Figure 3. The definition of the bond ellipticity is illustrated by the experimental $\rho(\mathbf{r})$ contour maps, showing the charge density in the plane perpendicular to the bond path at the Si–Si BCP of the $^1_\infty[Si]$ zigzag chains (left) and at the Ca–Si_a BCP (right). ε values larger than zero are a measure of the deviation from a cylindrical charge distribution $\rho(\mathbf{r})$ along a bond path: $\varepsilon = \lambda_1/\lambda_2 - 1$ (with $\lambda_1 < \lambda_2 < 0$). λ_i are the eigenvalues of the corresponding eigenvectors $\mathbf{v}_1$ and $\mathbf{v}_2$ of the Hessian matrix of $\rho(\mathbf{r})$; see Ref. [21] for further details.

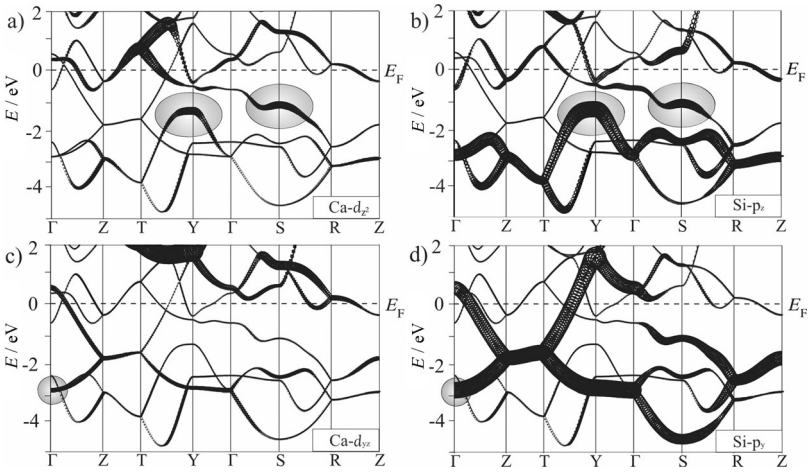

Figure 4. Fat band plots of a) Ca d_{z^2}, b) Si p_z, c) Ca d_{yz}, d) Si p_y states. The site- and state-projected band structure is shown in the energy range from −5 to 2 eV; lower energies are omitted for clarity. The mixing of the Ca d and Si p orbitals as discussed in the text has been highlighted by gray shaded ellipses.

Figure 4 and the Supporting Information, Figure S12, and these reveal that all of the bands of predominant Si p_y character are characterized by large dispersions and are crossing E_F (−5 to 2 eV relative to E_F) along the directions Γ→Z and T→Y of the *k* path as depicted in Figure 4d. Based on the chosen local coordinate system (Figure 2a) with the *y* axis (parallel to the crystallographic *a*-axis) pointing out of the plane defined by the $^1_\infty$[Si] zigzag chain (Figure 1a), the p_x and p_z orbitals of the Si atoms are orientated within the plane and mix with the s states by forming sp^2 hybrids (Supporting Information, Figure S12). Thus, the Si p_y orbitals are available to form delocalized π-bonds, which are a prerequisite for the metallic behavior of CaSi.

Furthermore, the Ca atoms also appear to be part of the delocalized π system of the $^1_\infty$[Si] moieties as evidenced by the pronounced bond ellipticity of 0.13 [0.29] at the Ca-Si_a BCP[22] and the orientation of the major axis of curvature ($\mathbf{v}_2$) along the *y* axis of our reference coordinate system (Figure 3). The presence of this type of interaction is also revealed by band structure analyses, which identify the mixing of the Ca d_{yz} and Si p_y states in the valence bands in the vicinity of the *Γ* point (Figure 4c,d). Inspection of the corresponding crystal orbital (Figure 5d) reveals that the Si p_y states not only accomplish the Si–Si π-interactions but also contribute to the (weakly pronounced) Si→Ca π donation within the $^1_\infty$[Si] zigzag chains. As a consequence, the Ca atoms are embedded in the π systems of the $^1_\infty$[Si] zigzag chains and do not only act as the source of the delocalized electrons but also enhance the delocalized character of this band. This observation is also in line with the significant d-orbital population of approximately 0.3 electrons at the calcium atom,[23] as obtained from the LAPW calculations.

The physical properties and bonding peculiarities of CaSi therefore contradict its classification as salt-like intermetallic compound as part of the Zintl–Klemm concept. Accordingly, the Ca–Si interactions are not of primarily ionic character but should be more precisely described by a combination of a highly polar Si→Ca σ donation and a somewhat weaker Si→Ca π donation component (Figure 5). The polar nature of the σ (Si→Ca) component is supported by the rather long Ca–Si bond and the positive value of the Laplacian ($\nabla^2\rho(\mathbf{r}_c) = 0.48$ [0.87] e Å^{-5}) at the Ca–Si BCP (Supporting Information, Table S9). However, the density accumulation at the Ca–Si_a BCP of $\rho(\mathbf{r}_c) = 0.15$ [0.13] e Å^{-3} is remarkably large and the integrated atomic charges of the Ca cations and Si anions (± 1.28 *e* [± 1.25 *e*]) deviate clearly from the ideal value of ± 2 *e* requested by the Zintl–Klemm concept. Also, the $G(\mathbf{r})/\rho(\mathbf{r})$ ratio is significantly smaller than unity (0.38 [0.52] Hartree e^{-1}) at the Ca–Si BCP and supports the weak but noticeable covalent character of the Ca–Si bond.[24]

The interplay of both Ca–Si bonding components is unequivocally revealed by the deformation density, $\Delta\rho(\mathbf{r})$, and the negative Laplacian of the total electron density, $L(\mathbf{r}) = -\nabla^2\rho(\mathbf{r})$, in the local *xz* and *yz* reference plane at the Ca atom (Figure 2 and 5). Figure 2a–c and 5a show the typical density signatures in the valence shell of the Ca atom, which are inherently linked with the presence of the Si(p_z)→Ca(d_{z^2}) σ donation. Indeed, the nodal structure and shape of the Ca $3d_{z^2}$ type orbital is mimicked by the four local $\Delta\rho(\mathbf{r})$ and $L(\mathbf{r})$ maxima in the valence shell of the calcium atom in the *xz* plane (Figure 2).[21b,25] Inspection of the corresponding $L(\mathbf{r})$ distribution in the *yz* reference plane reveals, however, that only the valence charge concentration opposite to the Ca–Si bond (denoted $CC_{Ca}(1)$ in Figure 2c and 5b) represents a true maximum in the three-dimensional $L(\mathbf{r})$ maps, while the other three charge concentrations at the Ca atom in the *xz* plotting plane of Figure 2c represent merely (3, +1) critical points (saddle points).

The relationship between the $L(\mathbf{r})$ pattern in the valence shell of the Ca atom and the molecular (crystal) orbital picture is depicted in Figure 5b–d, which outline how the Si→Ca π donation component is reflected by the $L(\mathbf{r})$ maps by the

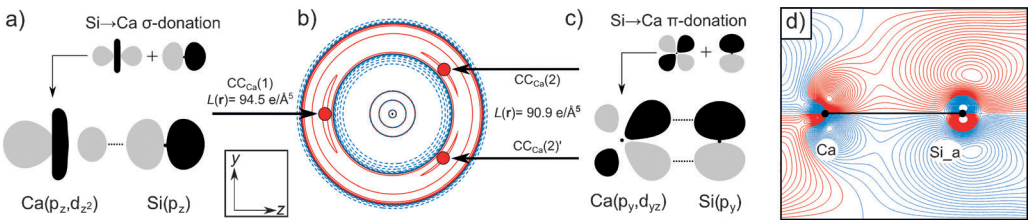

Figure 5. a), c) Orbital mixing diagrams illustrating the Si→Ca σ-donation and the Si→Ca π-donation component in the *yz* reference plane. b) Fine structure of the theoretical $L(\mathbf{r}) = -\nabla^2\rho(\mathbf{r})$ map at the Ca atom in the *yz* reference plane; contour lines as given in Figure 2c. d) Contour map of the respective crystal orbital at the Γ-point in steps of 0.005 e Bohr^{-3}.

presence of two charge concentrations in the valence shell of the Ca atom ($CC_{Ca}(2)$ and $CC_{Ca}(2)'$) and of the Si atom (see also the Supporting Information, Figures S10, S11).

To conclude, our combined experimental and theoretical charge density analysis of CaSi primarily supports the basic Zintl–Klemm concept by identifying the presence of predominant covalent Si–Si interactions in the complex polymeric anion. However, the Ca–Si bonds in the $^1_\infty$[Si] zigzag chain plane cannot be solely described by ionic interactions. Indeed, the present study provides for the first time clear experimental evidence that the cations in Zintl phases might be part of the covalently connected anionic substructures.[26] The chemical bonding scenario displayed by CaSi is therefore appropriately described by taking into account highly polar Si→Ca σ donation and somewhat weaker Si→Ca π donation components. Thus, the Ca atoms are embedded in the π system formed by the $^1_\infty$[Si] zigzag chains and the partial covalency of the Ca–Si bonds contributes to the delocalized character of the conduction band. This is in line with the results of band structure analyses showing the mixing of the $Ca(d_{yz})$ with the Si p_y states that contributes to the Si→Ca π donation within the $^1_\infty$[Si] zigzag chains. Accordingly, the integrated atomic charges of the Ca cations and Si anions (± 1.28 e [± 1.25 e]) clearly deviate from the ideal value of ± 2. Hence, the partial covalent character of the Ca–Si bonds appears be the physical origin of the remarkable metallic properties of CaSi.

Received: October 11, 2013
Published online: February 12, 2014

Keywords: band structure analysis · charge density · metals · Zintl phases · Zintl–Klemm concept

[1] a) E. Zintl, J. Goubeau, W. Dullenkopf, *Z. Phys. Chem. Abt. A* **1931**, *154*, 1–46; b) E. Zintl, A. Harder, *Z. Phys. Chem. Abt. A* **1931**, *154*, 47–91.
[2] E. Zintl, W. Dullenkopf, *Z. Phys. Chem. Abt. B* **1932**, *16*, 195–205.
[3] E. Zintl, *Angew. Chem.* **1939**, *52*, 1–6.
[4] *Zintl Phases*: *Principles and Recent Developments*, *Vol. 139* (Ed.: T. F. Fässler), Springer, Heidelberg, **2011**.
[5] W. Klemm, *Proc. Chem. Soc. London* **1958**, 329–341.
[6] F. Laves, *Naturwissenschaften* **1941**, *29*, 244–255.
[7] H. Schäfer, B. Eisenman, W. Müller, *Angew. Chem.* **1973**, *85*, 742–760; *Angew. Chem. Int. Ed. Engl.* **1973**, *12*, 694–712.
[8] G. Grube, A. Schmidt, *Z. Electrochem.* **1936**, *42*, 201–209.
[9] R. Nesper, *Angew. Chem.* **1991**, *103*, 805–834; *Angew. Chem. Int. Ed. Engl.* **1991**, *30*, 789–817.
[10] F. Wang, G. J. Miller, *Inorg. Chem.* **2011**, *50*, 7625–7636.
[11] The structural model of CaSi was first developed by Hellner and afterwards reinvestigated by Rieger and Parthé (orthorhombic, space group *Cmcm*, $a = 4.559$, $b = 10.731$, $c = 3.890$ Å, $Z = 4$. E. Hellner, *Z. Anorg. Allg. Chem.* **1950**, *261*, 226–236; W. Rieger, E. Parthé, *Acta Crystallogr.* **1967**, *22*, 919–922.
[12] P. Manfrinetti, M. L. Fornasini, A. Palenzona, *Intermetallics* **2000**, *8*, 223–228.
[13] The planar $^1_\infty$[Si] chain in CaSi has a bond and torsion angle of 104.889(6)° and 180°, respectively, whereas for gray Se, a helix-like structure is observed with corresponding angles of 102.39° and 106°, respectively, see D. R. McCann, L. Cartz, *J. Appl. Phys.* **1972**, *43*, 4473–4477.
[14] a) M. Affronte, O. Laborde, G. L. Olcese, A. Palenzona, *J. Alloys Compd.* **1998**, *274*, 68–73; b) O. Bisi, L. Braicovich, C. Carbone, I. Lindau, A. Iandelli, G. L. Olcese, A. Palenzona, *Phys. Rev. B* **1989**, *40*, 10194–10209.
[15] a) R. F. W. Bader, *Atoms in Molecules*: *A Quantum Theory*, Oxford University Press, Oxford, **1994**; b) R. F. W. Bader, *Chem. Rev.* **1991**, *91*, 893–928.
[16] a) For details on synthesis and characterization, see the Supporting Information. Crystal data for CaSi: $M_r = 68.16$, 100(2) K with $Ag_{K\alpha}$ radiation ($\lambda = 0.56087$ Å): metallic gray crystal (dimensions $0.052 \times 0.108 \times 0.119$ mm^3), orthorhombic, space group *Cmcm*, $a = 4.5516(2)$, $b = 10.7002(4)$, $c = 3.8869(1)$ Å, $V = 189.30(1)$ Å^3; $Z = 4$, $F(000) = 136$, $D_{calc} = 2.392$ g cm^{-3}, $\mu = 1.71$ mm^{-1} for a total of 14349 reflections yielding 1235 unique reflections. The high-resolution data set for the 100 K data provided 100% completeness in $6.0° < 2\theta < 103.2°$ ($\sin\theta_{max}/\lambda = 1.397$ Å^{-1}). The deformation density was described by a multipole model (Ref. [16b]) with spherical harmonics multiplied with Slater-type radial functions with energy-optimized exponents (Ref. [16c,d]) using the XD program (Ref. [16d]). Topological analyses of the experimental density was accomplished in the framework of the Quantum Theory of Atoms in Molecules (QTAIM; Ref. [15]). The refinement of 25 parameters against 1154 reflections ($F_o > 3\sigma(F_o)$, $\sin\theta_{max}/\lambda = 1.397$ Å^{-1}) converged to $R_1 = 0.0110$, $wR_2 = 0.0196$ and a featureless residual density map with minimum and maximum values of −0.296/0.185 e Å^{-3}($\sin\theta/\lambda \le 1.0$ Å^{-1}); b) N. K. Hansen, P. Coppens, *Acta Crystallogr. Sect. A* **1978**, *34*, 909–921; c) E. Clementi, D. L. Raimondi, *J. Chem. Phys.* **1963**, *38*, 2686–2689; d) A. Volkov, P. Macchi, L. J. Farrugia, C. Gatti, P. Mallinson, T. Richter, T. Koritsanszky, *XD2006 (version 5.42)—a Computer Program for Multipole Refinement*, *Topological Analysis of Charge Densities and Evaluation of Intermolecular Energies from Experimental or Theoretical Structure Factors*, **2006**.
[17] G. Celotti, D. Nobili, P. Ostoja, *J. Mater. Sci.* **1974**, *9*, 821–828.
[18] The small estimated ESD values are an inherent consequence of the high-resolution conditions of this experimental study and do not fully account for systematic errors of the diffraction experiment and/or insufficiencies of the employed multipolar model.
[19] a) D. Cremer, E. Kraka, *Angew. Chem.* **1984**, *96*, 612–614; *Angew. Chem. Int. Ed. Engl.* **1984**, *23*, 627–628; b) D. Cremer, E. Kraka, *Croat. Chem. Acta* **1984**, *57*, 1259–1281.
[20] A. Fischer, D. Tiana, W. Scherer, K. Batke, G. Eickerling, H. Svendsen, N. Bindzus, B. B. Iversen, *J. Phys. Chem. A* **2011**, *115*, 13061–13071.
[21] a) W. Scherer, P. Sirsch, D. Shorokhov, G. S. McGrady, S. A. Mason, M. G. Gardiner, *Chem. Eur. J.* **2002**, *8*, 2324–2334; b) W. Scherer, P. Sirsch, D. Shorokhov, M. Tafipolsky, G. S. McGrady, E. Gullo, *Chem. Eur. J.* **2003**, *9*, 6057–6070.
[22] If not specified otherwise, the Ca–Si_a bond as denoted in Figure 1a will be our reference Ca–Si bond and the symmetry label "a" will be therefore skipped in the following.
[23] The d-orbital population was estimated solely from contributions within the muffin-tin sphere of Ca.
[24] P. Macchi, D. M. Proserpio, A. Sironi, *J. Am. Chem. Soc.* **1998**, *120*, 13429–13435.
[25] G. S. McGrady, A. Haaland, H. P. Verne, H. V. Volden, A. J. Downs, D. Shorokhov, G. Eickerling, W. Scherer, *Chem. Eur. J.* **2005**, *11*, 4921–4934.
[26] The presence of covalent Au–Ba and Au–Ge cation–anion interactions has been earlier predicted by theoretical studies, that is, recently in the clathrate $Ba_8Au_{5.3}Ge_{40.7}$; see: H. Zhang, H. Borrmann, N. Oeschler, C. Candolfi, W. Schnelle, M. Schmidt, U. Burkhardt, M. Baitinger, J.-T. Zhao, Y. Grin, *Inorg. Chem.* **2011**, *50*, 1250–1257.

